VII International Conference on Computational Methods in Marine Engineering
MARINE 2017
M. Visonneau, P. Queutey and D. Le Touzé (Eds)

RANS-based full-scale power predictions for a general cargo vessel, and comparison with sea-trial results

A.R. STARKE[*], K. DRAKOPOULOS[†], S.L. TOXOPEUS[*] AND S.R. TURNOCK[†]

[*] Maritime Research Institute Netherlands (MARIN)
2, Haagsteeg, P.O. Box 28, 6700 AA Wageningen, Netherlands
e-mail: b.starke@marin.nl, www.marin.nl

[†] University of Southampton
University Road, SO17 1BJ, Southampton, UK
email: drakopuloskostas@gmail.com, www.soton.ac.uk

Key words: CFD, power prediction, full-scale validation

Abstract. Blind self-propulsion predictions for the 2016 LR Workshop on Ship Scale Hydrodynamic Computer Simulation have been carried out to simulate the full scale performance of a self-propelled ship in ballast. The single screw ship of 11542 tonnes had been scanned in drydock so the computational model used the actual as operated hull form. It will be shown that using a hybrid RANS-BEM method, the predicted ship speeds at self-propulsion are over-estimated by 0.17-0.28 knots compared to the trial data. The various aspects that influence the accuracy of the direct prediction of power and RPM using CFD are critically discussed.

1 INTRODUCTION

CFD tools are being used more and more extensively in practical ship hull form design and in the prediction of the power and RPM. An evaluation of the progress in this field can e.g. be found in the assessment of the Gothenburg 2010 Workshop and the proceedings of the subsequent workshop in Tokyo, 2015. The cases in that workshop series, however, are until now restricted to model scale. This is motivated by the lack of publicly available full-scale trial data, including the ship and propeller geometries. In the summer of 2016 Lloyd's Register announced the organization of a hydrodynamics workshop with blind numerical predictions of ship-scale power. The main objective of the workshop was to compare these results with available sea trials measurements, and to assess and develop the capabilities of the numerical tools at ship scale. In the present paper we will discuss our contributions to that workshop.

2 DESCRIPTION OF THE TEST CASE

The ship under consideration is a general cargo vessel built in 1994 in Poland, with a gross weight of 11542 tonnes. The ship is equipped with one four-bladed, right handed, fixed-pitch propeller. Some of the particulars of the ship and the propeller have been listed in Table 1. The reference location for the propeller centre was 2689 mm ahead of the aft perpendicular and 3147 mm above the base. Immediately preceding the trials the vessel was dry-docked and the hull and propeller cleaned. Following that the hull, rudder and propeller were 3D laser

scanned to obtain an accurate geometric representation of the in-service geometry. However, some modifications to the scanned geometry had to be carried out to make them suitable for viscous-flow computations. Many more details of the test case can be found in [1].

Table 1: Particulars of the ship and the propeller.

Symbol	Description	Value	Unit
L_{pp}	Length between perpendiculars	138	m
B	Breadth	23	m
T	Design draught	8.5	m
T_f	Forward draught	4.899	m
T_a	Aft draught	5.597	m
S	Wetted surface area	3727	m^2
V_s	Design speed	14	kts
ρ	Water density (at 26.5 ^oC)	1010	kg/m^3
ν	Dynamic viscosity	$0.88397x10^{-6}$	m^2/s
D	Propeller diameter	5.2	m
P(0.7 R)/D	Pitch ratio	0.6781	-

3 COMPUTATIONAL METHODS

The viscous-flow method used for the majority of computation reported in this paper is PARNASSOS, a code developed and used by MARIN and IST [2,3]. It solves the discretised Reynolds-averaged Navier-Stokes (RANS) equations for a steady, 3D incompressible flow around a ship's hull. Various eddy-viscosity turbulence models are available. For all computations in this paper, the one-equation turbulence model by Menter [4] was used, extended with a correction for the longitudinal vorticity by Dacles-Mariani et al. [5].

The discretisation is of finite-difference type. All terms in the momentum and continuity equations are discretised by second or third-order accurate difference schemes. PARNASSOS can handle body-fitted, generally non-orthogonal HO-type grids, either single or multi-block structured.

The momentum and continuity equations are solved in fully coupled form. Therefore, the continuity equation need not be recast in a pressure correction or pressure Poisson equation, but can simply be solved as it is. After discretisation and linearisation, the three momentum equations and the continuity equation give rise to a matrix equation containing 4*4 blocks, which is solved using preconditioned GMRES. This fully coupled solution has been found to be robust and quite insensitive to the mesh aspect ratio. This allows solving the discretized equations on extremely contracted grids close to the wall. As a result, wall functions are not necessary, not even at full scale. More details about the solution strategy can be found in [3].

PARNASSOS makes use of a surface-fitting method to determine the free surface, based on the steady iterative formulation which, contrary to almost all other RANS/FS methods, involves no time-dependent terms. The problem is solved by an iterative procedure, instead of by time integration. This iteration is based on the use of a combined free-surface condition that is obtained by substituting the wave elevation from the dynamic boundary condition into

the kinematic boundary condition for the free surface. Together with the dynamic condition it describes exactly the same problem as the original set of conditions.

For the analysis of the flow past the propeller, use is made of a boundary element method (BEM) that solves the incompressible potential flow equations for lifting and non-lifting bodies. The method, designated PROCAL, is being developed within MARIN'S Cooperative Research Ships (CRS) for the unsteady analysis of cavitating propellers operating in a prescribed ship wake. It has been validated for open water characteristics, shaft forces, sheet cavitation inception and extent and hull pressure fluctuations. The code is a low order BEM that solves for the velocity disturbance potential. Initial validation studies and details on the mathematical and numerical model can be found in [6,7].

The steady RANS solver and the unsteady boundary element method are coupled in the following way:

- First a RANS computation is made for the case without propeller. This provides the resistance and the nominal wake field at the propeller plane.
- Then, a first propeller computation is made using the BEM, for the propeller in this wake field at the prescribed rotation rate. This provides a thrust and loading distribution. The unsteady loading distribution, in a ship-fixed coordinate system, is averaged in time for all blade positions to produce a steady, but axially, circumferentially and radially non-uniform force distribution. This is interpolated to the RANS grid.
- We restart the viscous-flow computation from the previous solution and impose this loading distribution as a force field acting on the flow. This yields a new total wake field, from which we then subtract the induced velocities coming from the BEM to obtain the first estimate of the effective wake field.
- We iterate between both methods until the thrust and torque coefficients and the effective inflow to the propeller do not change any more.

4 COMPUTATIONAL DOMAIN AND GRID GENERATION

The computational domain extended from the inflow boundary, located $1L_{pp}$ in front of the bow, to the outflow boundary, $1.5L_{pp}$ behind the transom. The lateral outer boundary is a quarter of a cylinder with axis $y=z=0$ and radius $1L_{pp}$. At this boundary tangential velocities and pressure found from a potential-flow computation are imposed. In the resistance computations only the starboard side of the ship was taken into account, due to symmetry considerations. This mesh consisted of 512 x 200 x 52 cells in the streamwise, girthwise and wall-normal directions, respectively. Approximately 200 cells in the streamwise direction were distributed along the hull. The cells in the wall-normal direction were contracted strongly towards the hull, to capture the gradients in the boundary layer, resulting in y^+ values below 0.4 in all computations. For the power predictions the mesh was mirrored to port side as well, resulting in a mesh with 10.6M cells.

5 RESISTANCE PREDICTIONS

Resistance computations have been performed at seven different speeds. Three of those,

namely 8, 10 and 12 knots, were three of the cases that were requested for the resistance predictions at the workshop. Two more speeds, namely 9 and 13 knots, resulted from the power predictions at the workshop. These values served as indications of the ship speeds that were obtained from the trials at the given RPM's. During the workshop the actually obtained ship speeds were revealed and for two of those, namely 9.25 and 11.58 knots, resistance and power predictions have been performed afterwards as well.

Convergence levels that could be obtained in the resistance computations turned out to be speed dependent. At the lower speeds, 8, 9 and 9.25 knots, but also at 13 knots both the RANS-equations and the free-surface updates in our steady iterative approach were well converged. Maximum changes in the pressure coefficients and the dimensionless velocities at any point in the domain had dropped below 1×10^{-5}; maximum changes in the free surface elevation were less than 1 mm. For these cases any significant influence of the iterative errors on the solutions can safely be disregarded. For the remaining three speeds, 10, 11.58 and 12 knots, convergence was somewhat more cumbersome to achieve. Maximum changes in the solutions were typically 1-2 orders of magnitude larger than for the other speeds. The largest changes in the solutions consistently occurred near the free surface, either near the bow or near the rudder. As will be discussed in more detail later, the solutions showed clear indications of the occurrence of an overturning bow wave at most of the speed range, while as a consequence of the loading conditions during the trials the rudder protruded through the free surface at all speeds. The difficulties in the convergence behavior are likely to be related to these features. Table 2 presents the main flow parameters for the resistance computations.

Table 2: Main parameters of the flow.

Ship speed (V_s)		Reynolds number (Rn)	Froude number (Fn)
knots	m/s	-	-
8	4.116	6.43×10^8	0.112
9	4.630	7.23×10^8	0.126
9.25	4.759	7.43×10^8	0.129
10	5.144	8.03×10^8	0.140
11.58	5.957	9.30×10^8	0.162
12	6.173	9.64×10^8	0.168
13	6.688	1.04×10^9	0.182

Figure 1 presents the resistance values that have been obtained. The red diamonds correspond to the CFD predictions, containing the contribution of the hull and the rudder only. The blue squares are the same values augmented with a correlation allowance, C_A, to account for the features that have not been taken into account in the simulations. Finally the dashed line corresponds to an estimated resistance curve for the present test case that is based on MARIN's statistical prediction method (DESP).

At lower speeds the computations show a smooth increase in the resistance with increasing speed, practically parallel to the DESP curve. At higher speeds the behavior of the predicted resistance is more irregular. Compared to the DESP curve the resistance at 11.58 knots seems to be somewhat high, while the opposite holds for the two highest speeds. Recalling that the convergence levels of the computations in the range between 10 and 12 knots were the least, one might be tempted to fit the resistance curve through the three lowest and the highest point.

That then would lead to a curve that runs slightly less steep than the one from DESP. However, it has to be emphasized that the comparison with the statistical method can only be used as indicative, not as a validation. Further confidence in the resistance predictions thus has to come from mutual comparison of numerical results. When doing so for the results that were provided at the workshop, however, no less than 11-16 per cent spreading was reported between the resistance values, after disregarding the highest and lowest values. This indicates that the full-scale CFD resistance predictions are not yet sufficiently mutually consistent, and there is work to be done.

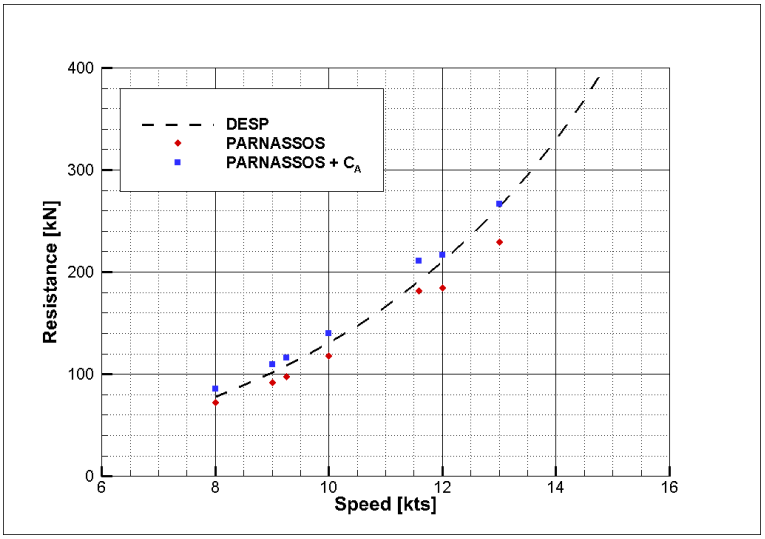

Figure 1: The resistance curve.

As mentioned above, the CFD predictions (the red diamonds in the figure) contain the contributions of the hull and the rudder only. Added to that should be resistance estimations of firstly the bilge keels and anodes that prior to the workshop were removed from the hull geometry after the 3D laser scan. This was done because the quality of these scanned surfaces was judged to be insufficient. Their contributions may be a few per cent of the bare-hull resistance. Secondly the resistance of the superstructure is needed. That might be included in the simulation, or determined in a separate simulation for the superstructure only, or estimated using the expression by Bowden-Davison, as recommended by the ITTC. In the proceedings of the workshop an added air resistance of up to seven per cent is reported. Thirdly at full scale the resistance increase due to surface roughness cannot be ignored. This can be included through an empirical relation of e.g. Townsin, or numerically through the adaptation of the boundary conditions in the turbulence model. As additional input these two methods then require the specification of the mean apparent amplitude (MAA) or an equivalent sand grain roughness height. For the present ship the measured MAA, after cleaning the hull, was reported to vary over the hull in the range 70-270 μm. At the design speed, according to Townsin's formula, this would add something between 2-8 per cent to the bare-hull resistance.

These, and other contributions that are not further discussed here, easily add 10-20 per cent to the bare-hull resistance. At MARIN all the contributions mentioned above are typically

collected into a single correlation allowance that is added to the full-scale bare-hull resistance. For the present ship this allowance has been determined as $C_A = 0.456 \times 10^{-3}$. As the predicted resistance coefficients lie in the range $2.37 - 2.75 \times 10^{-3}$, this indeed corresponds to a resistance increase of 15-20 per cent (the blue squares in the resistance curve). These values will be used later on in this paper to evaluate the self-propulsion points.

Apart from the comparison of the total resistance, it can be very worthwhile to compare the predicted frictional resistance coefficients with well-known friction lines, such as for instance the ITTC-'57 model-ship correlation line, the Grigson line or the more recently derived numerical friction lines [8]. As the displacement effect of the ship results in an increase of the velocity along most of the ship, it can be expected that the frictional resistance of the ship is higher than the frictional resistance of an equivalent flat plate. How much exactly is not known, but values close to, or even below, the friction lines can be regarded as indications of numerical errors. Indeed, such values occurred at the present workshop, but also at the 2015 Tokyo Workshop. In the discussions following that workshop, it was mentioned that one of the likely causes of under-estimated friction is the (improper) use of wall functions. For our present results, where no wall functions have been used, Figure 2 compares the predicted friction coefficients with several friction lines. The dash-dotted black line in the figure corresponds to an eight per cent upward shift of the numerical friction lines corresponding to Menter's one-equation turbulence model, which is the model used in these simulations. Thus we find a friction coefficient that is consistently 8 per cent above that line, and that over the entire speed range. Obviously, a different percentage is found when comparing to another friction line.

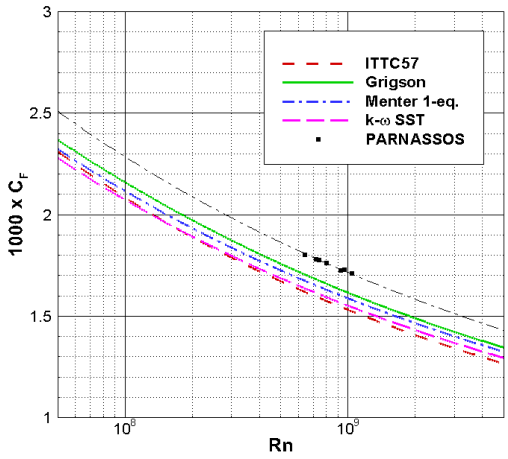

Figure 2: Comparison of the predicted friction coefficients with several friction lines.

We now consider some features that characterize the wave pattern and flow field around the ship. Figure 3 illustrates the predicted bow wave system at various speeds, colored with the axial velocity component at the free surface. With increasing speed a pronounced bow wave develops, with the highest wave crest located at some distance in front of the ship. With increasing wave height, and thus with increasing ship speed, the axial velocity in the top of the wave crest decreases; from $u/V_s = 0.22$ at 9.25 knots, to $u/V_s = 0.09$ at 11.58 knots and at 12 knots the axial velocity has become negative. This, together with the steepness of the bow

wave, is a clear indication that the bow wave will be over-turning in reality. It is evident that an over-turning bow wave cannot be a solution in the surface-fitting method that has been implemented in PARNASSOS. And this may also explain why good convergence was found to be more difficult to achieve in this region at the higher speeds. For comparison the bottom-right of Figure 3 shows a result obtained with ReFRESCO (http://www.refresco.org), which uses a volume-of-fluid (VOF) method to model the free surface. Shown is an iso-surface through the points where the air volume fraction equals one half. Here the occurrence of an over-turning bow wave in reality is even more convincing.

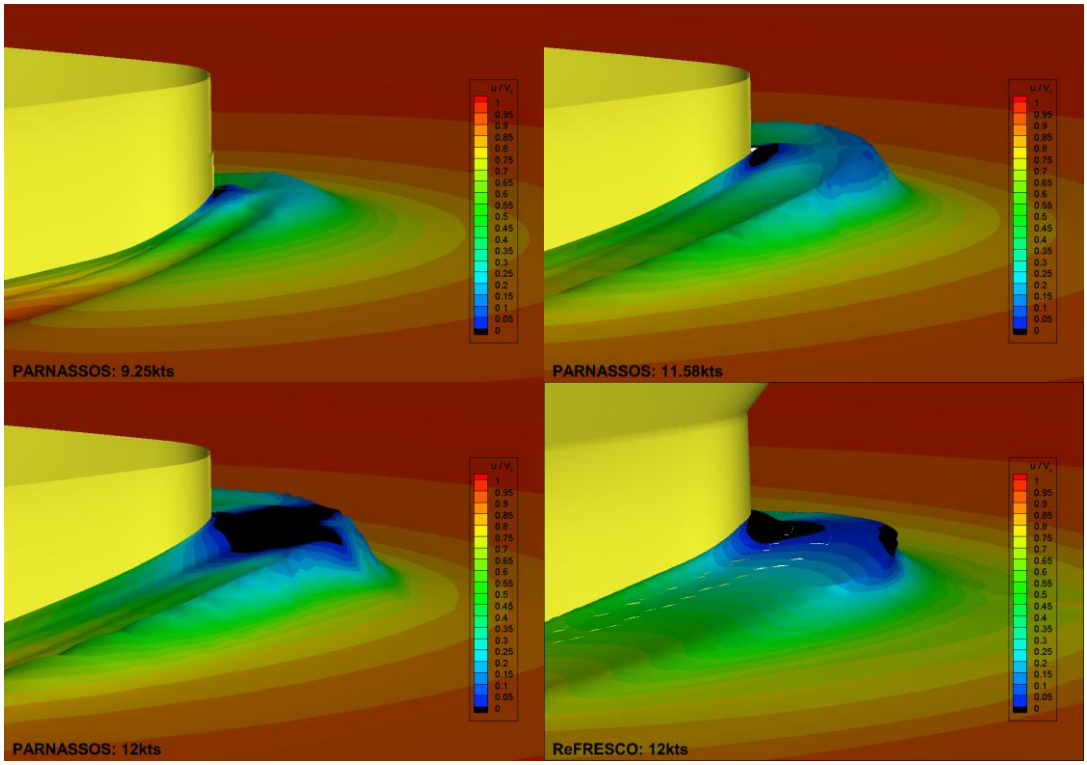

Figure 3: Development of the bow-wave system.

Figure 4 shows the axial velocity field near the stern for the lowest and the highest speeds considered here. Due to the specific loading condition during the trials (T_f = 4.988 m., T_a = 5.597 m. compared with a design draught of T = 8.5 m.) the stern and the transom of the ship are lifted well above the free surface, also when sailing. At all but the highest speed, the waterline ends just above the ship's gondola. The top part of the rudder is above the water surface over the entire speed range. Consequently the rudder creates its own wave pattern with diverging waves coming from the leading and the trailing edge. At lower speeds the trailing-edge wave was found to be quite short with low velocities in the top, possibly given rise to the formation of a short spilling breaker in reality. At higher speeds (higher Froude numbers) the top of this wave shifted aft and became less steep.

It can also be seen from Figure 4 that there will be not much clearance between the tip of the propeller blades and the free surface at the present loading condition.

To finish the discussion of the resistance computations Figure 5 presents the nominal wake

fields at the propeller plane for the 8 and 13 knots cases. Both fields can be characterized by the presence of two longitudinal vortices in the bottom half of the discs. Note that at the design condition these vortices are most likely located in the top half of the disc, where they are used to make the axial velocity field more homogeneous. But under the present loading condition they have shifted downwards. The axial velocity field at 8 knots shows somewhat higher velocities in the top of the disc and below the shaft than at 13 knots, but for the rest there is not much difference between them. The nominal wake fractions integrated over these discs have been found to change from $1-w_{nom} = 0.52$ at 8 knots to $1-w_{nom} = 0.49$ at 13 knots.

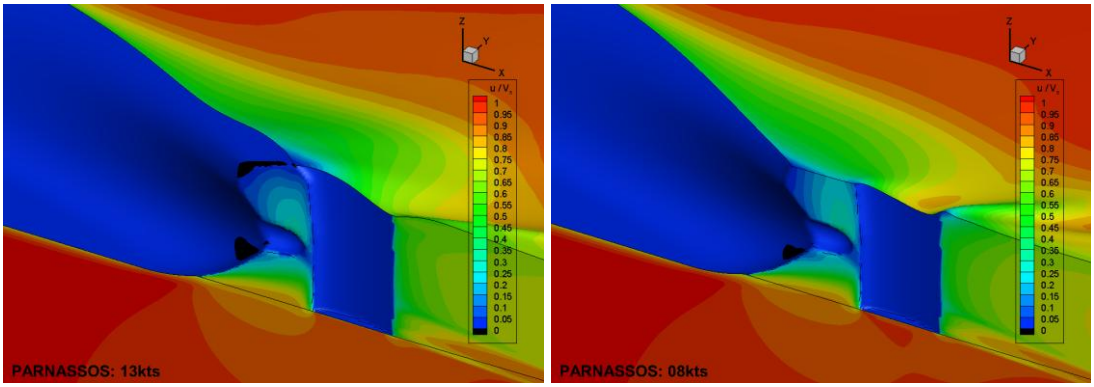

Figure 4: Detail of the flow fields near the stern.

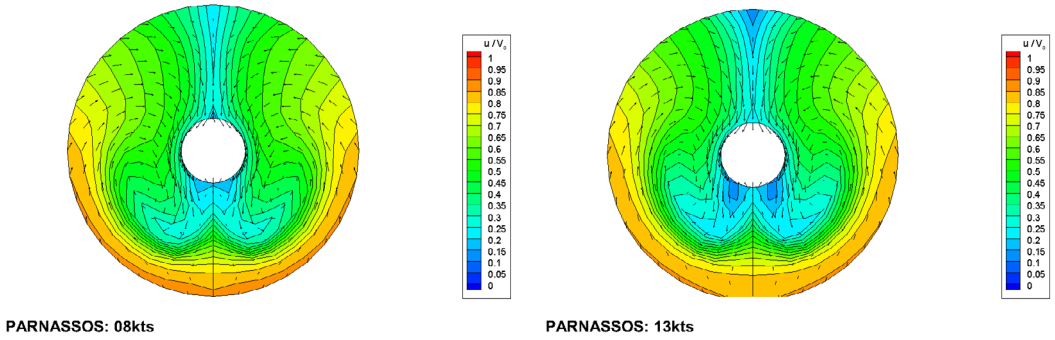

Figure 5: The nominal wake fields at 8 and 13 knots.

6 PROPULSION PREDICTIONS

For the self-propulsion predictions at the workshop it was requested to determine the ship speeds that were obtained given the shaft speeds recorded during the trials, namely 71.6, 91.1 and 106.4 RPM. However, such an approach would require an iterative adjustment of the inlet velocity in the RANS computations, which can be computationally expensive. The approach adopted by most participants at the workshop, and also by us, was to perform a number of computations at fixed ship speed and RPM, and determine the self-propulsion point from those. Indications of the obtained ship speeds at the RPM's mentioned above were provided prior to the workshop as 9, 12 and 13 knots, respectively. Here we will report our results for the two lowest shaft speeds. For efficiency reasons the approach we have adopted for these computations is as follows:

- First we restarted the RANS free-surface computations from the resistance results, imposing the axial loading distribution from the propeller only (after averaging). In such a way port-starboard symmetry was preserved and the first iterations for the propeller-hull interaction could efficiently be performed for one side of the ship only.
- Secondly, we mirrored the solution from starboard to port side and restarted the computations including the radial and tangential loading of the propeller as well. Thus the asymmetry of the axial loading and the influence of the propeller swirl on the flow field were taken into account.

Our contributions to the workshop included the cases with the shaft speeds of 71.6 and 91.1 RPM. The corresponding simulation were performed at the indicated ship speeds of 9 and 12 knots, respectively. During the workshop the actually achieved ship speeds from the trial results were given, being 9.25 knots at 71.6 RPM and 11.58 knots at 91.1 RPM. Computations using these conditions have been performed after the workshop, and results of all four simulations will be discussed here.

Table 3: Main results for the analysis of the power predictions.

V_s [kts]	n [Hz]	$R+C_A$ [kN]	R_T+C_A [kN]	T [kN]	Q [kNm]	K_T	$10K_Q$	P_D [kW]	$1-w_{eff}$	t
9	1.193	109.44	150.61	174.3	109.3	0.166	0.200	819.8	0.549	0.236
9.25	1.193	116.07	157.82	170.7	107.6	0.162	0.197	807.3	0.546	0.245
11.58	1.518	211.10	258.98	270.1	169.6	0.159	0.192	1618	0.552	0.177
12	1.518	216.76	273.50	268.5	168.7	0.158	0.191	1609	0.535	0.211

Table 3 lists the main parameters that are required to analyze the power predictions, augmented with the corresponding resistance values taken from the previous section and the thrust deduction fraction. First consider the imbalance between the thrust, T, and the resistance force acting on the hull in propulsion plus the correlation allowance, $R_T + C_A$. At 9 knots we found a higher thrust than resistance, which would lead to an acceleration of the ship. At 12 knots the predicted thrust was somewhat lower than the resistance, and thus the ship would decelerate. The trial data indicate that the ship speed at 71.6 RPM is indeed higher than 9 knots, namely 9.25 knots, and at 91.1 RPM lower than 12 knots, namely 11.58 knots. However, also in the new computations that have been performed at exactly those conditions, we do not find a balance between thrust and resistance; in both cases the thrust exceeds the resistance by 11-13kN, indicating an increase of the ship speed compared to the trial data. To determine the magnitude of the ship speed at self-propulsion point we use the open-water diagram of the propeller, shown at the left-hand side of Figure 6. This diagram gives a relation between the thrust coefficient and the advance coefficient J. If it is assumed that the effective wake fraction is constant than $J = (1-w_{eff})V_s/(nD)$ will vary linearly with the ship speed, which for a small difference in speed is a reasonable assumption. From an estimated increase in speed, a corresponding decrease of the thrust can then be calculated. An estimation for the new value of the resistance that has to be overcome can then be obtained from the resistance at the higher speed (from the resistance curve in Figure 1) plus the thrust deduction times the new thrust.

For example, at 9.25 knots we found a thrust of T = 170.7kN and a thrust coefficient K_T =

0.162. In the open-water diagram this corresponds to an advance coefficient of J=0.4062. We estimate an increased ship speed as $V_s^* = 9.53$ knots. This gives a new advance coefficient of $J = (V_s^*/V_s) \times J^* = 0.4185$. From the open-water diagram we read a new thrust coefficient $K_T^* = 0.156$. Thus the thrust changes to $T^* = (K_T^* / K_T) \times T = 165.2$kN. From the resistance curve we read the resistance at the new speed, $R^* = 125.3$kN. The total resistance force that has to be overcome by the thrust then equals $R_T^* = R^* + tT^* = 165.8$kN. And now R_T^* and T^* are practically equal. Thus to obtain self-propulsion in the present computations at 71.6 RPM, the ship speed should be increased to 9.53 knots, 0.28 knots higher than determined from the trials. The delivered power at that speed can then be determined as $P_D = 765.5$kW. Performing a similar analysis for the 11.58 knots case results in an increase of the ship speed with 0.17 knots to 11.75 knots, at a delivered power of $P_D = 1570$kW.

A comparison of these points with the trial data is given at the right-hand side of Figure 6.

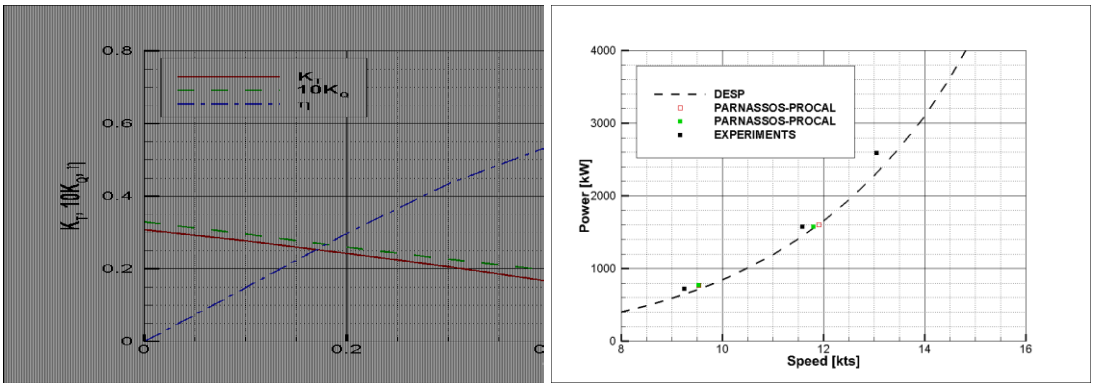

Figure 6: The open-water diagram (left) and the speed-power curve (right).

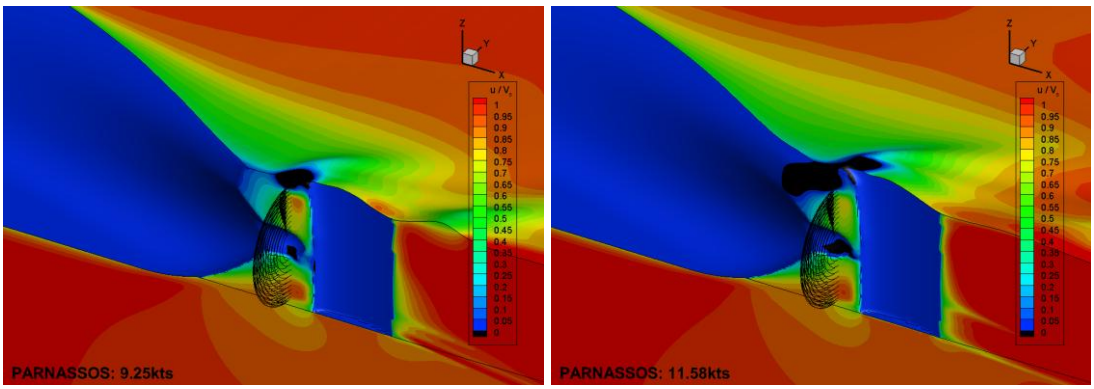

Figure 7: Detail of the flow fields near the stern at the starboard part of the domain.

The results that have been submitted to the workshop are indicated by red, open squares, and the new results by green, solid squares. For the lowest RPM both computations (at 9 and 9.25 knots) result in the same estimated speed and power at self-propulsion, as was to be expected. At the higher RPM, however, the computations at 11.58 and 12 knots do not result in the same self-propulsion point, indicating that there must be some inconsistencies between these computations. From Table 3 it can for instance be read that the difference in the effective wake fraction and the thrust deduction is much larger for these two cases, compared to the 9 and 9.25 knots cases. Finally from Figure 7 it can be seen that the power predictions

are also complicated by the flow field. At the left-hand side (9.25 knots case) a clear region with reversed flow (indicated by black contour flooding) at the free surface is present above the propeller in the solution. At 11.58 knots, the right-hand side of the figure, this region has extended upstream to the stern.

6 DISCUSSION

Figure 8 shows the speed-power predictions of all participants of the workshop, reproduced from [2] with kind permission of the organizers. For each of the three cases the spreading of the predicted ship speed at given RPM is more than 1 knot, indicating that in general these predictions are not yet sufficiently accurate, or well-controlled. Evidently, numerous error sources can be the cause of the observed spreading: discretization errors due to insufficient grid resolution or time stepping, iterative errors due to lack of convergence, influence of turbulence models on the predicted resistance and propeller inflow, the influence of wall functions, etc. In the absence of any experimental data on e.g. the resistance or the wake field, this spreading can only be reduced by careful analysis of the numerical results and mutual comparison of numerical results.

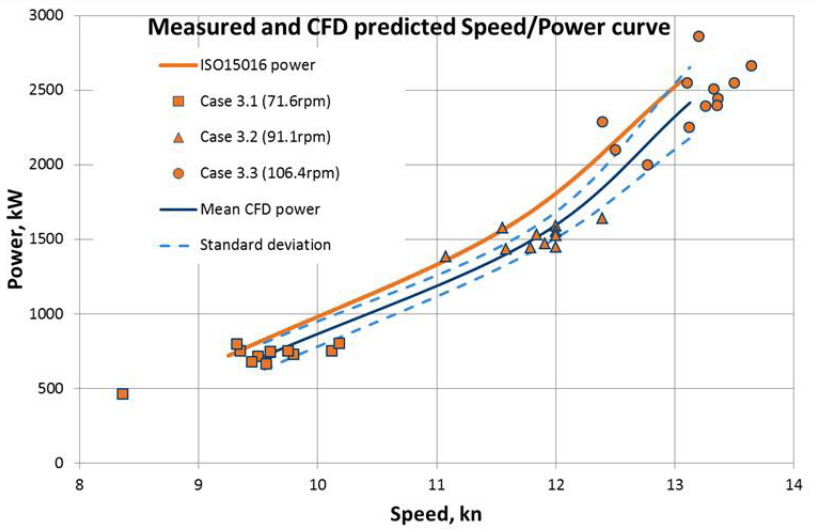

Figure 8: Measured and CFD predicted speed-power curve for the three cases of the workshop.

However, it can also be that the present test case gives a somewhat negative view on the capability of CFD to predict power and RPM at full scale. We have illustrated in our paper that due to the specific loading conditions at the trials, flow features occur that complicate the CFD predictions, such as bow-wave breaking and flow reversal at the free surface just above the propeller. These are less likely to occur at the design draught of the ship, so it may well be that the accuracy of the predictions and the consistency of the results increase if the same exercise would be performed at the design conditions. But then we are obviously lacking any trial data for validation.

On the other hand, looking at the figure it can also be seen that the majority of the CFD results are consistently located below the experimental speed-power curve, resulting in an over-prediction of the ship speed compared to the trials. Or, equivalently, one could claim that

the resistance of the ship is consistently under-estimated. Realizing that the correlation allowance that has to be added to the predicted resistance of the ship is in general determined for newly-built ships, it might also be that the resistance of this ship, having served for over twenty years, is higher than expected. If that would be true, most CFD results would be in better agreement with the trial data.

6 CONCLUSIONS

Using a hybrid RANS-BEM method we have over-estimated the ship speed at two self-propulsion points by 0.17-0.28 knots, compared to the trial data. Although that is judged to be somewhat too high to be acceptable in practical design projects, the CFD was complicated by the flow features caused by the specific loading condition at the trials, which are not likely to occur at the design conditions.

The frictional resistance of the ship exceeded the value of the corresponding numerical friction line in our computations by 8 per cent, consistently over the entire speed range (8-13 knots).

There is a significant spreading in the results of all participants. A detailed evaluation and mutual comparison of all aspects in the resistance and propulsion computations is required to reduce this spreading to more acceptable levels in future workshops.

ACKNOWLEDGEMENT

This research is partially funded by the Dutch Ministry of Economic Affairs.

REFERENCES

[1] Ponkratov, D. *Proceedings of the 2016 Workshop on Ship Scale Hydrodynamic Computer Simulation*. Lloyds Register Ref. 8428, Feb. 2017.

[2] Hoekstra, M., "*Numerical simulation of ship stern flows with a space-marching Navier Stokes method*", PhD Thesis, Technical University of Delft, Oct. 1999.

[3] Van der Ploeg, A., Eça, L. and Hoekstra, M., "*Combining accuracy and efficiency with robustness in ship stern flow calculation*", 23rd Symp. Naval Hydrodynamics, Val de Rueil, France, Sept. 2000.

[4] Menter, F.R., "Eddy-*viscosity transport equations and their relation to the k-ε model*", Journal of Fluids Engineering,Vol. 119, pp. 876-884, 1997.

[5] Dacles-Mariani, J., Zilliac, G.G., Chow, J.S. and Bradshaw, P., "*Numerical/experimental study of a wingtip vortex in the near field*", AIAA Journal, Vol. 33, Sept. 1995, pp. 1561 - 1568.

[6] Vaz, G., Bosschers, J., "*Modelling of three dimensional sheet cavitation on marine propellers using a boundary element method*", 6th Int. Symp. on Cavitation CAV2006, Wageningen, NL, Sept. 2006.

[7] Vaz, G., "*Modelling of sheet cavitation on hydrofoils and marine propellers using boundary element methods*", PhD Thesis, Instituto Superior Técnico, Lisbon, Portugal, 2005.

[8] Eça, L. and Hoekstra, M., (2008), "*The numerical friction line*", J. Mar. Sci. Technol., May 2008.